ACS APPLIED MATERIALS & INTERFACES

Research Article

www.acsami.org

One-Pot Synthesis of Dendritic Gold Nanostructures in Aqueous Solutions of Quaternary Ammonium Cationic Surfactants: Effects of the Head Group and Hydrocarbon Chain Length

Deping Huang, Yuanyuan Qi, Xiangtao Bai, Lijuan Shi, Han Jia, Dongju Zhang, and Liqiang Zheng*

Key Laboratory of Colloid and Interface Chemistry, Shandong University, Ministry of Education, Jinan, 250100, P. R. China

Supporting Information

ABSTRACT: Hierarchical, three-fold symmetrical dendritic gold was prepared in an aqueous solution of the quaternary ammonium cationic surfactant dodecyltrimethylammonium bromide (DTAB). Similar surfactants with different head groups and hydrocarbon chain lengths were also used for comparison. Two-fold and one-fold symmetrical dendritic gold nanostructures were obtained in N-dodecyl-N-methylpyrrolidinium bromide (C_{12}-MPB) and dodecyltriethylammonium bromide (DTEAB) aqueous solutions, respectively. Longer hydrocarbon chain lengths were unfavorable for the formation of dendritic nanostructures. The interaction energies between the individual surfactants and Au (111) plane were calculated using molecular dynamics simulations. Based on a series of contrast experiments and molecular dynamics simulations, the possible growth mechanism and fabrication process of the dendritic structures were proposed. The DTAB-capped, three-fold gold dendrites exhibited good surface-enhanced Raman scattering (SERS) sensitivity toward rhodamine 6G (R6G), indicating their potential for use in SERS-based detections and analysis. This work provides a simple and effective strategy for fabricating dendritic gold nanostructures in aqueous solutions.

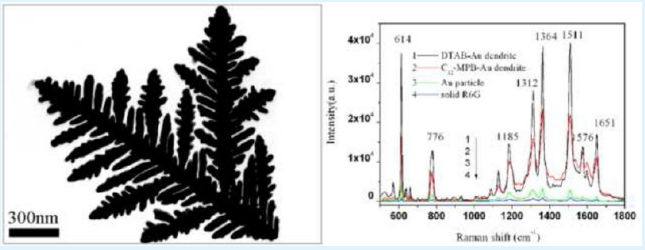

KEYWORDS: *dendritic gold nanostructures, ammonium cationic surfactant, DTAB, head groups, hydrocarbon chain length, SERS*

1. INTRODUCTION

Fractal dendritic morphologies of metal nanoparticles have attracted great attentionbecause of their potential applications in advanced materials science and their abilities to serve as platforms to obtain fundamental understanding of the preparation of these structures with unique properties through self-assembly methods.[1] Particularly, star-shaped dendritic gold nanostructures have been reported frequently because of their unique morphologies, properties, and potential applications in surface-enhanced Raman scattering (SERS), catalysis, and electrocatalysis.[2−4] Various methods have been developed to prepare dendritic gold nanostructures in recent years. Electrochemical[2a,5] and galvanic exchange[6] methods are traditional ways to prepare dendritic nanostructures. The colloid chemical method[7] (also known as the wet chemical method) is another powerful way to fabricate dendritic nanostructures.

In terms of the formation mechanism, most dendritic nanostructures are the result of either the growth of anisotropic particles or directional interactions between isotropic particles in the medium.[1b] Some of these structures are generated by a nonequilibrium process due to fractal growth on the molecular scale.[1b,8] Diverse morphologies could form in a nonequilibrium, kinetically controlled synthesis.[9] Star-shaped dendritic nanostructures could be obtained at high driving force, i.e., far from equilibrium.[10] Because the kinetically controlled reaction occurs far from equilibrium, a slight variation in the reaction conditions could amplify the differences in the surface energies and change the growth rates of individual facets. In the colloid chemical method, the use of different capping agents could further amplify the differences between each surface by selective adsorption.[11]

In the colloid chemical method, additives usually play a very important role in controlling the morphologies of the nanostructures. Various additives, such as polymers,[3a,12] biomacromolecules,[13] thiol-containing reagents,[14] amino-containing reagents,[15] surfactants[16] and ionic species and supermolecules,[17] have been used in the preparation of nanomaterials. Replication of Au on certain templates was recently proved to be an effective way to fabricate flower-like Au nanostructures.[17c,d] Amino-containing reagents seem to have particular effects on the formation of dendritic nanostructures. Gold dendrites have been fabricated by employing vapor-phase polymerization of pyrrole, which acted as a stabilizer, onto a solution-cast film of block polymer ionomers.[18] Polyvinylpyrrolidone (PVP), a polymer with pyrrolidone groups, can be adsorbed on metal surfaces through charge-transfer interactions between the pyrrolidone rings and metal atoms and can thereby act as a stabilizer.[19] PVP-capped dendritic Ag, Pt and Au

Received: June 9, 2012
Accepted: August 9, 2012
Published: August 9, 2012

   dx.doi.org/10.1021/am301040b | ACS Appl. Mater. Interfaces 2012, 4, 4665−4671

nanostructures have been obtained previously.[12] Tang et al.[2c] prepared PVP-capped dendritic gold nanoparticles with ammonium formate (AF) as a reducing agent. They found that AF is the origin of the dendritic Au particles, whereas PVP is a stabilizer. According to the literature, quaternary ammonium cationic groups are frequently involved in the formation of dendritic nanostructures. Poly(diallyldimethylammonium chloride) (PDDA), a polymer with a quaternary ammonium group, has been used to prepare three-fold single-crystalline dendritic gold nanostructures by Han et al.[4] [3-[[(Heptadecafluorooctyl)sulfonyl]amino]-propyl]trimethylammonium iodide ($CF_3(CF_2)_7$-SO_2NH-$(CH_2)_3N^+(CH_3)_3I^-$, HFOTAI), a surfactant with a quaternary ammonium cationic group, acts as both a reducing agent and an assembling agent to form dendrimer-like gold nanostructures.[20] Recently, we have successfully prepared planar two-fold gold dendrites with the assistance of the bolaform surfactant decane-1,10-bis(methylpyrrolidinium bromide) ([mpy-C_{10}-mpy]Br_2), which is also a capping agent containing a quaternary ammonium cationic headgroup.[21]

Typically, alkyltrimethylammonium bromide (C_nTAB) is an important series of quaternary ammonium cationic surfactants that are mostly used as capping agents in the preparation of nanomaterials.[16,22,23] Their quaternary ammonium cationic head groups and long hydrocarbon chains may lead to the formation of anisotropic crystals by selectively adsorbing on different crystal planes.[22] Dendritic silver[22a] nanostructures have been synthesized in a cetyltrimethylammonium bromide (CTAB) and sodium dodecyl benzyl sulfonate (SDBS) mixed surfactant solution. Hexatrimethylammomium bromide (HTAB) has been used to prepare three-dimensional gold dendrites via a seeding growth method.[22b] It was found that the quantity of seeds was very important in determining the morphologies of the final products. Huang et al.[23] prepared planar three-fold gold dendrites in a dodecyltrimethylammonium bromide (DTAB) and β-cyclodextrin (β-CD) mixed solution. They demonstrated that the molar ratio of DTAB to β-CD was a very important factor influencing the dendritic nanostructures. Further, they found that rodlike branches were formed instead of dendrites in a 2.5 mM pure DTAB solution, which they explained to be a result of fewer DTAB molecules adsorbed on the gold surface. However, we found that at a lower concentration of the DTAB (2.0−2.4 mM) solution, well-defined, three-fold dendritic gold nanostructures could be formed.

Herein, we report a one-pot synthesis of dendritic gold nanostructures grown along the ⟨211⟩ direction in a DTAB aqueous solution. The effects of the head groups, hydrocarbon chain length and concentration of surfactants on the morphologies of the products were investigated. The interaction energies between the surfactants and the Au (111) plane were calculated using molecular dynamics simulations. A possible growth mechanism was proposed, and the influence of each factor on the growth mechanism was discussed in detail. The well-defined dendritic gold nanostructures exhibited great enhancement in the surface-enhanced Raman scattering (SERS) toward R6G, indicating they have potential for use in SERS-related detections and analysis. The as-prepared dendritic gold nanostructures are easy to collect and soluble in water, which greatly facilitates their use in practical applications.

2. EXPERIMENTAL SECTION

2.1. Chemicals. N-Methylpyrrolidine, 1-bromododecane, cetyltrimethylammonium bromide (CTAB), tetradecyltrimethylammonium bromide (TTAB), and dodecyltrimethylammonium bromide (DTAB) were bought from Aladdin Chemistry Co., Ltd. 1-Bromohexadecane, tetrachloroauric acid tetrahydrate ($HAuCl_4{\cdot}4H_2O$, AR) and L-ascorbic acid (AA, 99.7%) were purchased from Shanghai Chemical Reagent Co., Ltd., and all reagents were used without further purification. N-Alkyl-N-methylpyrrolidinium bromide (C_n-MPB, n = 12, 14, 16)[24] and dodecyltriethylammonium bromide (DTEAB)[25] were synthesized according to the literature with details given in the Supporting Information.

2.2. Preparation and Characterization of Dendritic Gold Nanostructures. In a typical synthesis, a DTAB (120 μL, 0.1 M) aqueous solution and $HAuCl_4$ (21 μL, 0.048 M) were added to 4.6 mL of water at ambient temperature. The bright yellow precursor complex was formed immediately. Then, ascorbic acid (300 μL, 0.1 M) was added to the precursor solution, and the mixture was allowed to sit for 24 h. The products were collected by centrifugation and washed several times with water. The as-prepared gold nanostructures were characterized by scanning electron microscopy (SEM, JEOL JSM-7600F) together with energy-dispersive X-ray spectroscopy (EDS), transmission electron microscopy (TEM, JEOL JEM-100CX II, 100 kV) and high-resolution TEM (HRTEM, JEM-2100).

2.3. Numerical Simulation. Molecular dynamics (MD) simulations were performed in the canonical (NVT) ensemble (constant atom number, volume, and temperature) to calculate the interaction energies between the surfactants and Au (111) planes. The simulations and structural analysis are similar to a previously reported method.[26,27] To obtain the interaction energy for the gold-surfactant system, we established three models: (1) a three-dimensional model consisting of the Au (111) crystal plane and a certain amount of surfactant molecules on the gold surface, (2) the Au (111) plane only and (3) the surfactants only. All simulations were performed using the Discover Module in Materials Studio 4.4. The COMPASS force field was used to calculate the interaction potential energy. All systems were subjected to energy minimization before the MD simulations. The NVT simulations lasted for 50 ps with a time step of 1 fs. Simulation data were collected in the last 20 ps. The interaction energies between different surfactants (DTAB, C_{12}-MPB, DTEAB) and the Au (111) plane were calculated.

2.4. SERS Measurements. SERS measurements were carried out using a confocal microprobe Raman spectrometer (Jobin-Yvon HR800). The excitation wavelength was 633 nm, and the power was 20 mW. The spectrum was collected with a 50× objective to focus the laser on a spot approximately 1 μm in diameter. The data acquisition time was 5 s for one accumulation. A solid R6G sample was prepared by drop casting 100 μL of a 1.0×10^{-4} M RG6 aqueous solution onto a quartz substrate. Other samples were prepared by drop casting 100 μL of the gold substrates and 100 μL of 1.0×10^{-4} M R6G. The samples were measured several times at different positions to obtain average intensities.

3. RESULTS AND DISCUSSION

3.1. Structural Characterization of the Three-Fold Gold Dendrites. TEM and SEM images of the dendritic gold nanostructures obtained in the DTAB aqueous solution are shown in Figure 1. The gold dendrites are approximately 1−2 μm, and every single dendrite has several trunks reaching in different directions (Figure 1a, b). Each fully developed trunk is approximately symmetric and has secondary side branches. The secondary branches are also symmetric and have integral tertiary leaves. The whole dendrite is hierarchical and three-fold nanostructures. The XRD patterns of the dendritic gold nanostructures (shown in Figure 2) exhibit sharp diffraction peaks corresponding to the {111}, {200}, {220}, {311} and {222} planes (Joint Committee on Powder Diffraction Standards (JCPDS) No. 04−0784), indicating that the

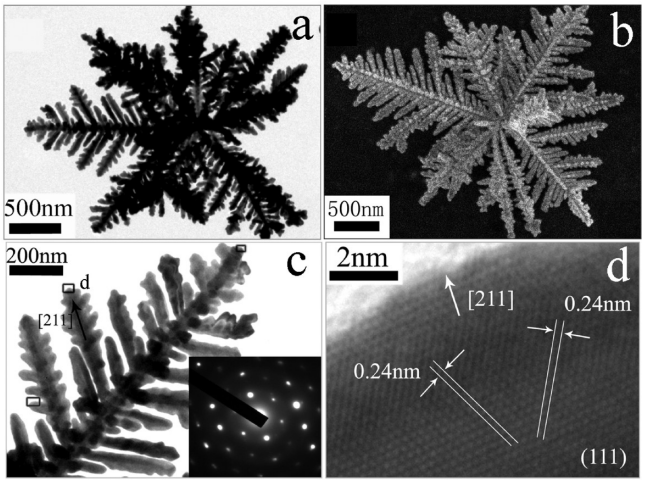

Figure 1. (a) TEM, (b) SEM, and (c, d) HRTEM images of dendritic gold nanostructures prepared in a $HAuCl_4$ aqueous solution containing DTAB (R = 12) (the inset in c shows the corresponding SAED pattern).

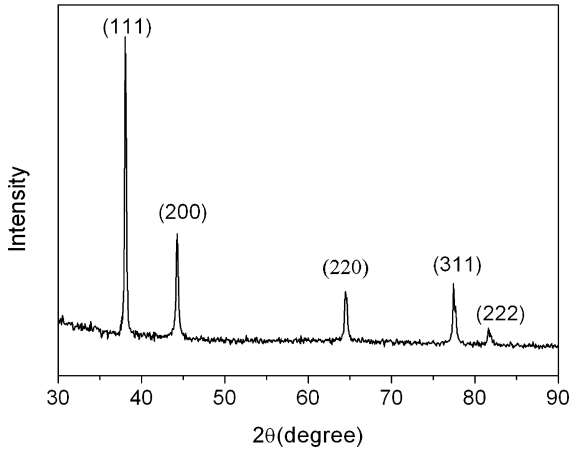

Figure 2. XRD patterns of dendritic gold nanostructures prepared in a $HAuCl_4$ aqueous solution containing DTAB.

dendrites are face-centered cubic (fcc) Au crystals. The related energy-dispersive X-ray spectroscopy (EDS) pattern (see Figure S1 in the Supporting Information) confirms that the dendritic nanostructures are composed of gold. HRTEM images and the selected area electron diffraction (SAED) pattern of the gold dendrites are shown in Figure 1c, d. The SAED pattern shows a perfect hexagonal pattern, which verifies that the dendrites contain single-crystalline {111} faces. The hexagon diffraction spots inside attributed to the formally forbidden (1/3) {422} reflections,[24] which can be indexed to the $[\bar{1}11]$ zone axis of cubic gold and demonstrate that the gold dendrites are single crystals with the (111) plane as the top surface. The HRTEM images of the second-order branch (shown in Figure 1d) show clear lattice fringes with a d spacing of 0.24 nm and also confirmed that the gold dendrites are single crystals with a (111) plane and grew along the ⟨211⟩ direction. The HRTEM images of the first- and tertiary-order branches (see Figure S2 in the Supporting Information) show the same lattice fringes and growth direction as the second-order branch, which means that all three branch orders have (111) planes and grow along the ⟨211⟩ direction.

Which part of the DTAB surfactant, the headgroup or the hydrocarbon chain, is essential for the formation of dendritic nanostructures? The effects of the headgroup and hydrocarbon chain length were studied by comparing different surfactants.

3.2. Effects of the Head Groups. Quaternary ammonium cationic C_{12}-MPB and DTEAB were used to fabricate gold nanostructures and compare the effects of the headgroup with DTAB. TEM and SEM images of the dendritic gold nanostructures obtained using the three different surfactants are shown in Figure 3. The dendritic structures obtained in C_{12}-

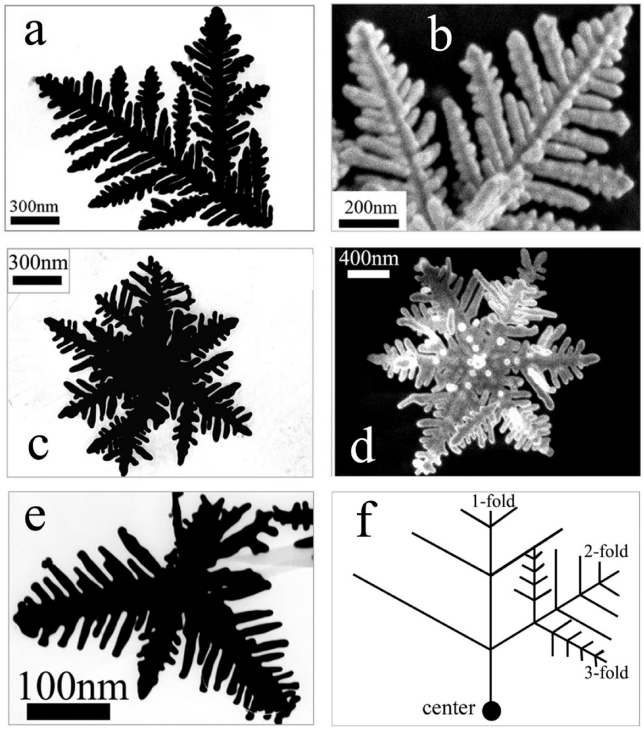

Figure 3. (a, c, e) TEM and (b, d) SEM images of dendritic gold nanostructures prepared in an aqueous solution containing (a, b) DTAB, (c, d) C_{12}-MPB and (e) DTEAB; (f) illustration of the orders of leaves in the dendritic nanostructures described in this article.

MPB and DTEAB have similar spatial architectures as the DTAB-capped structures, but the trunks are less developed. The gold dendrites are also approximately 1 μm and have hierarchical branching structures. The dendrite obtained in C_{12}-MPB has several trunks, and all fully developed trunks have symmetrical secondary side branches. Only a few secondary branches have regular tertiary branches. The dendrites obtained in DTEAB only have secondary branches. The SAED pattern and HRTEM images of the gold dendrites prepared in the C_{12}-MPB aqueous solution (shown in Figure S3a, b in the Supporting Information) demonstrate that the dendritic nanostructures are single-crystalline Au grown along the ⟨211⟩ direction, which is similar to the nanostructures prepared in the DTAB aqueous solution. The XRD pattern (see Figure S3c in the Supporting Information) exhibits sharp diffraction peaks corresponding to the {111}, {200}, {220}, {311}, and {222} planes, as also observed in the XRD pattern of the DTAB-capped dendrites.

The definition of fold as described in this article is shown in figure 3f. We concluded that surfactants with different quaternary ammonium cationic head groups could affect the order of the dendritic nanostructures. The nanostructures

obtained in DTAB, C_{12}-MPB and DTEAB are three-, two-, and one-fold, respectively.

We found that surfactants with different head groups have different optimal concentrations for the formation of well-defined dendritic nanostructures. Figure 4 and Figures S4 and S5 in the Supporting Information show the nanostructures obtained under different concentration ratios of the surfactant to $HAuCl_4$ (R) for DTAB, C_{12}-MPB and DTEAB, respectively. For DTAB, only irregular nanoparticles were formed at rather low surfactant concentrations ($R < 3$). Simple one-fold dendrites with several branches were formed when the R value was increased to 6 (Figure 4b). Dendritic nanostructures with trunks and several side branches were formed when the R value was further increased to 9 (Figure 4c). The best R value to form three-fold dendritic nanostructures in the DTAB aqueous solution is 12 (Figures 1 and 4b), whereas in the C_{12}-MPB aqueous solution, this R value is approximately 20 (shown in Figure 3c, d). In the DTEAB aqueous solution, the products have well-defined, three-fold structures when the R value was 9 (Figure 3e). When the R value was increased to 30 or 50, the resulting dendritic structures deteriorated and were thick and short-branched (Figure 4e, f).

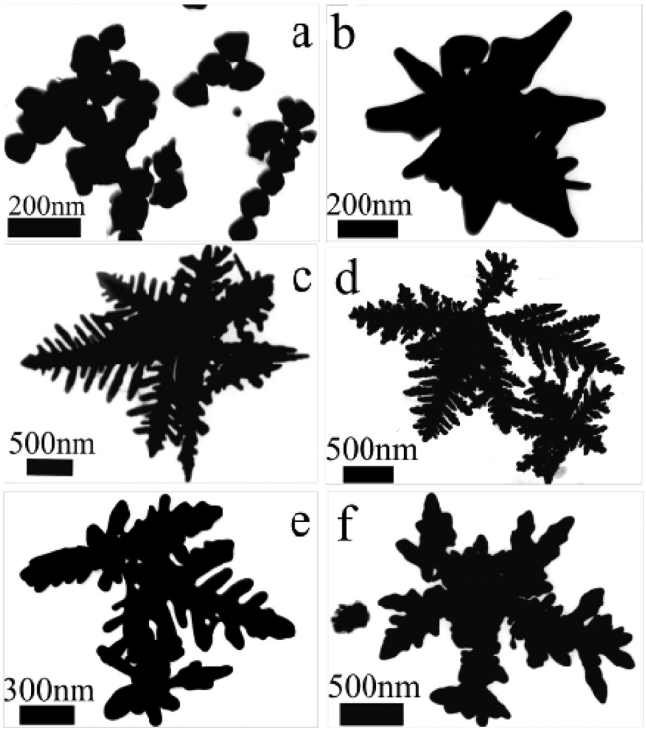

Figure 4. TEM images of dendritic gold nanostructures obtained using different R values of DTAB: (a) 3, (b) 6, (c) 9, (d) 12, (e) 30, (f) 50.

Therefore, the concentrations of the surfactants influence the final morphology of the nanostructures in the same way, but each surfactant has a different optimal R value for the formation of perfectly constructed dendritic nanostructures. The best R values for DTAB, C_{12}-MPB, and DTEAB to obtain dendritic nanostructures are 12, 20 and 9, respectively. The differences in the optimal R values might be due to the different sizes of the head groups, as discussed in detail in the Formation Mechanism section.

3.3. Effects of the Hydrocarbon Chain Length. To elucidate the influence of the hydrocarbon chain length on the dendritic structures formed, analogues of DTAB (TTAB, CTAB) and C_{12}-MPB (C_{14}-MPB, C_{16}-MPB) were used as capping agents to prepare gold nanostructures. We found that the length of the hydrocarbon chain can dramatically change the morphologies of the final products. The nanostructures obtained in the TTAB and C_{14}-MPB aqueous solutions were thick-branched structures (Figure 5a, b), while only irregular nanoparticles were formed in CTAB and C_{16}-MPB (Figure 5c, d). Obviously, DTAB and C_{12}-MPB, which have shorter hydrocarbon chains, are favorable for the formation of dendritic nanostructures, while the longer hydrocarbon chains inhibit the formation of dendritic nanostructures. The role of the hydrocarbon chain length during the formation of the dendrites will be discussed in the Formation Mechanism section.

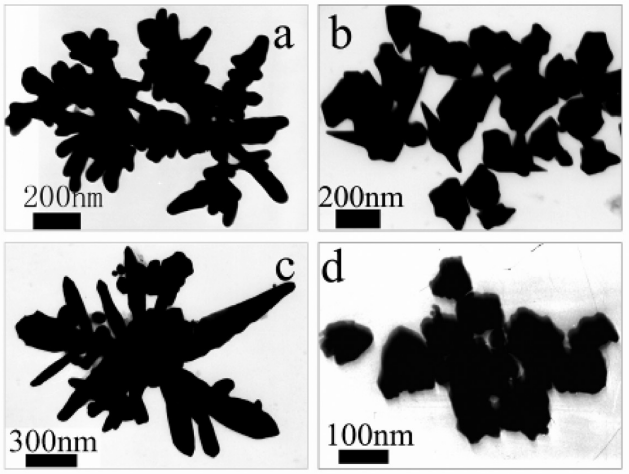

Figure 5. Gold nanostructures obtained in (a) TTAB, (b) CTAB, (c) C_{14}-MPB, and (d) C_{16}-MPB.

3.4. Formation Mechanism. The formation process is always a focus topic in research on dendritic nanostructures. It has been reported that star-shaped dendritic nanostructures could be obtained when the driving force is large (i.e., far from equilibrium[10]) through a nonequilibrium, kinetically controlled synthesis process. Kinetic control can be realized by substantially slowing down the precursor decomposition or reduction process.[15] Therefore, the formation of more complicated structures requires a higher driving force, i.e., a lower reaction or precursor decomposition rate.

Here, we present a possible formation mechanism for the dendritic nanostructures in this study. A schematic illustration of the dendritic nanostructure formation process is shown in Figure 6. First, the precursor complex of the quaternary ammonium cationic headgroup and $AuCl_4^-$ was formed through electrostatic interactions. When the reducing agents, AA, were added, $AuCl_4^-$ was slowly released from the complex and reduced to Au^0. Initially, Au^0 aggregated and formed Au nuclei, which were stabilized by the excess surfactant molecules adsorbing as a bilayer on the Au surface.[22d] The Au nuclei acted as seeds, which is similar to the process described by Lee et al.[22b] Those seeds became the growth centers of the dendrites. Continuous reduction created small Au nanoparticles dissolved into the solution. The growth continued as small particles diffused to and adsorbed on the Au nuclei. The kinetically controlled process was realized because of three key factors: (1) the weak reducing agent (AA) provided a slow reducing rate for the nonequilibrium, kinetically controlled process of anisotropic

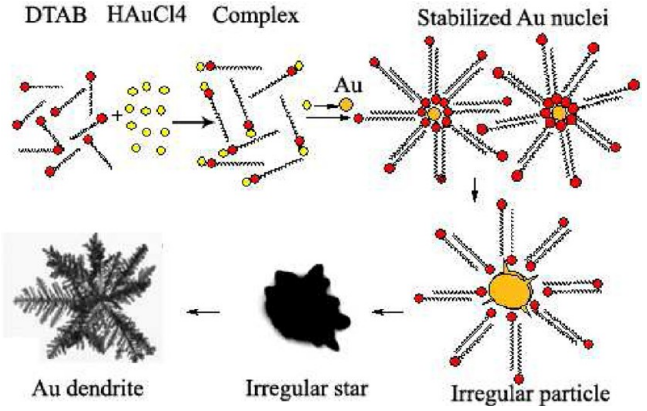

Figure 6. Schematic illustration of the dendritic nanostructure formation process in aqueous solutions containing quaternary ammonium cationic surfactants.

growth; (2) $AuCl_4^-$ formed a precursor complex with the surfactants and was slowly released after AA was added, further decreasing the reducing rate; and (3) small Au nanoparticles capped by the surfactant bilayer have a hydrophilic surface, making them soluble in aqueous solutions, and their stability depends on the hydrocarbon chains of the surfactants. Hence, these small gold nanoparticles were temporarily stable in the aqueous solution, which delayed the accumulation time and decreased the growth rate of the dendrites. As the driving force increases, the growth rate is governed by mass diffusion or heat transfer, and the growth surface becomes unstable in the diffusion field. Under this condition, a dendrite with a complicated periodic structure will be produced because of the competition between the promotion and suppression of the crystal growth.[28]

Because the kinetically controlled reaction occurs far from equilibrium, a small change in the reaction conditions could amplify the differences in the surface energies and the growth rates of individual facets.[11] In our case, DTAB, C_{12}-MPB, and DTEAB have the same hydrocarbon chain lengths, and the differences between their head groups were amplified. According to the kinetically controlled process, three-fold dendritic nanostructures require a slower reaction rate to form. During the experiments, we indeed noticed that when AA was added to the reaction solution, the yellow color of the DTAB/$AuCl_4^-$ precursor faded more slowly by approximately 10 s than that of the precursors formed with the other two surfactants, which directly confirmed the slower reaction rate in the DTAB aqueous solution. However, what causes the differences between these three surfactants? We hypothesized that the differences might due to the different interaction energies (U) of the surfactants with the Au (111) plane. The interactions of the surfactants with the gold surface were investigated using MD simulations. The interaction energies were calculated by the following equation[26]

$$U = E_{total} - E_{surface} - E_{saa}$$

where E_{total} is the total energy of the Au (111) crystal plane with adsorbed surfactants, $E_{surface}$ is the Au (111) plane energy without surfactants and E_{saa} is the energy of the surfactants without the Au (111) plane. A negative value indicates attractive interactions. The results of the MD simulations are shown in table 1. DTAB has the strongest interaction energy with the Au (111) plane, demonstrating that the strongest adsorption complex involves DTAB and Au (111) plane. We find that the stronger adsorption complex is favorable for the formation of dendritic nanostructures, which might due to the slower desorption hindering the growth of the Au crystal. In addition, the critical micelle concentration (CMC) values[25] of DTAB, C_{12}-MPB, and DTEAB are 15.0, 13.5, and 13.0 mM, respectively. Because they have same hydrocarbon chain length, the CMC values reveal the hydrophilicity of their head groups. DTAB has the highest CMC value, which indicates the greater hydrophilicity of its headgroup. The DTAB-capped nanoparticles, therefore, have the best stability and slowest growth rate, leading to the formation of three-order leaves in the DTAB aqueous solution.

Table 1. Calculated Interaction Energies (kcal mol^{-1}) between Surfactants with Different Head Groups and the Au (111) Plane

	DTAB	C_{12}-MPB	DTEAB
Au(111)	−338.97	−203.50	−164.96

The three surfactants have different appropriate concentrations for the formation of well-developed dendritic nanostructures. The minimum area (A_{min}) occupied per surfactant molecule at the air/water interface of DTAB and C_{12}-MPB were 63.2 nm^2 and 54.8 nm^2, respectively.[24] A smaller headgroup allows more surfactant molecules to be adsorbed on the Au surface due to decreased steric hindrance. An increase in the concentration of the surfactant cannot obviously influence the bilayer adsorption of the surfactant. Therefore, with the smallest headgroup, C_{12}-MPB has the highest optimal concentration (R = 20) for the formation of well-developed dendritic nanostructures. The headgroup of DTEAB is obviously larger than the other two surfactants; hence, only a few molecules could be adsorbed on the small nanoparticles side by side because of strong steric hindrance between the head groups. Consequently, DTEAB has the lowest optimal concentration for the formation of well-constructed dendritic nanostructures.

The length of the hydrocarbon chain greatly influences the morphology of the products. The CMC values of CTAB, TTAB, DTAB, C_{16}-MPB, C_{14}-MPB, and C_{12}-MPB are 0.93, 4.08, 14.80, 0.86, 3.30, and 13.50 mmol/L,[24] respectively. The CMC values reveal that increasing the hydrocarbon chain length significantly increases the hydrophobic effect of the hydrocarbon chains. In the present study, the DTAB and C_{12}-MPB molecules adsorbed on the Au surface as a bilayer to keep it stable and hydrophilic, and the small Au nanoparticles were thus effectively capped to prevent aggregation and reduce the growth rate of the dendrites. The gold nanoparticles capped with TTAB and C_{14}-MPB are not as stable as those capped with DTAB and C_{12}-MPB because of the stronger hydrophobic interactions of their long hydrocarbon chains. Thus, only thick-branched structures formed. The gold nanoparticles capped with CTAB or C_{16}-MPB aggregated immediately due to the strong hydrophobicity of their long hydrocarbon chains; hence, no dendritic nanostructures were obtained in the CTAB or C_{16}-MPB aqueous solution.

In summary, the head groups of the ammonium cationic surfactants determine the order of the dendritic nanostructures, whereas an appropriate hydrocarbon chain length is the critical factor for the formation of dendritic nanostructures in quaternary ammonium cationic surfactant aqueous solutions.

dx.doi.org/10.1021/am301040b | ACS Appl. Mater. Interfaces 2012, 4, 4665−4671

3.5. SERS Activity. Dendritic nanostructures have been reported to have great potential for applications as substrates in SERS.[29] Because sharp corners, edges and nanoscale gaps serve as SERS "hot spots",[30] dendritic gold nanostructures usually show very strong enhancement toward SERS. In the present study, the enhancement abilities of the as-prepared three- and two-fold nanostructures were investigated using R6G as a model molecule. The nanoparticles were prepared by reducing $HAuCl_4$ with $NaBH_4$ in a sodium citrate aqueous solution. Figure 7 shows the SERS spectra of R6G in the presence of two

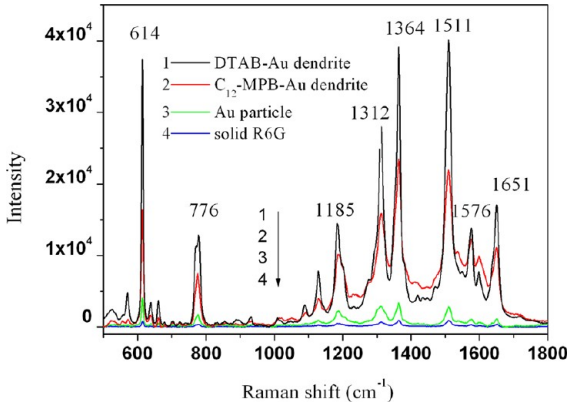

Figure 7. Raman spectrum of solid R6G and SERS spectra of R6G molecules adsorbed on the gold dendrites and nanoparticles (excitation wavelength 633 nm, acquisition time 5 s, R6G concentration 1.0×10^{-4} M).

dendrites and Au nanoparticles. For both dendrites, remarkably enhanced Raman peaks were observed. These peaks were assigned to the C−C stretching of the aromatic ring (1651, 1576, 10511, 1364 cm^{-1}), C−O−C stretching (1321 cm^{-1}), C−H in-plane bending (1185 cm^{-1}), C−H out-of-plane bending (776 cm^{-1}), and C−C−C ring in-plane bending (614 cm^{-1}).[31]

The magnitude of the enhancement factors (*EF*s) for R6G on the dendritic gold nanostructures was quantitatively evaluated using the following equation[32]

$$EF = (I_{SERS}/N_{ads})/(I_{bulk}/N_{bulk})$$

where I_{SERS} is the intensity of the enhanced spectrum, I_{bulk} is the intensity of the normal Raman spectrum of R6G, N_{bulk} is the number of R6G molecules in the bulk, and N_{ads} is the number of R6G molecules adsorbed on the surface of the substrates. The details of the calculation are shown in the Supporting Information. The *EF*s of the three gold substrates at 614, 1364, and 1511 cm^{-1} are listed in table 2.

Both of the dendritic gold substrates have much higher *EF*s than the Au nanoparticles, demonstrating their stronger enhancement abilities. The DTAB-capped, three-fold dendrites have stronger enhancement than the C_{12}-MPB-capped, two-fold dendrites, possibly because of the presence of more nanoscale junctions and tips in the three-fold dendrite, which act as "hot spots". The DTAB-capped, three-fold dendritic gold nanostructures might find a potential application in SERS-based technologies based on their high efficiency and facile preparation and the low expense of DTAB.

Table 2. SERS *EF*s of Dendritic Gold Nanostructures Capped with Different Surfactants and Gold Nanoparticles Calculated from the SERS Intensity Showmn in Figure 7

	EF values		
substrates	614 cm^{-1}	1364 cm^{-1}	1511 cm^{-1}
DTAB-Au dendrite	7.73×10^6	7.88×10^5	7.56×10^5
C_{12}-MPB-Au dendrite	6.80×10^5	4.71×10^5	4.13×10^5
Au particle	1.69×10^5	6.72×10^4	5.34×10^4

4. CONCLUSIONS

Three-fold dendritic gold nanostructures were obtained in aqueous solutions containing quaternary ammonium cationic surfactants. The capping agents could substantially affect the structures of the dendritic nanoparticles. Only two- and one-fold dendritic nanostructures can be obtained in C_{12}-MPB and DTEAB aqueous solutions due to the weak interaction energy between the head groups and Au (111) plane. Longer hydrocarbon chains are unfavorable for the formation of dendritic nanostructures. No dendrites have been obtained in CTAB or C_{16}-MPB aqueous solutions because of the strong hydrophobic interaction of the longer hydrocarbon chains. A possible formation mechanism for the dendritic nanostructures in aqueous solutions of quaternary ammonium cationic surfactants has been proposed. This work presents a simple, ultrafast and cheap way to prepare dendritic gold nanostructures in aqueous solutions using a small molecule as the capping agent. This method also provides a straightforward procedure to explore the formation mechanism of dendritic gold structures due to the simple structure of DTAB. Dendritic gold nanostructures exhibit high SERS sensitivity toward R6G and have potential for use as SERS substrates.

■ ASSOCIATED CONTENT

Ⓢ Supporting Information

Complete synthesis procedures for C_{12}-MPB and DTEAB, EDS spectra and HRTEM images of the dendritic nanostructures obtained in the DTAB and C_{12}-MPB aqueous solutions, TEM and SEM images of the nanostructures obtained using different concentrations of C_{12}-MPB and DTEAB, details for the SERS *EF* calculations. This material is available free of charge via the Internet at http://pubs.acs.org.

■ AUTHOR INFORMATION

Corresponding Author

* E-mail: lqzheng@sdu.edu.cn. Phone: +86-531-88366062. Fax: +86-531-8856470.

Notes

The authors declare no competing financial interest.

■ ACKNOWLEDGMENTS

The authors are grateful to the National Natural Science Foundation of China (50972080 and 91127017) and the National Basic Research Program (2009CB930101).

■ REFERENCES

(1) (a) Akcora, P.; Liu, H.; Kumar, S. K.; Li, Y.; Benicewicz, B. C.; Schadler, L. S.; Acehan, D.; Panagiotopoulos, A.; Pryamitsyn, V.; Ganesan, V.; Ilavsky, J.; Thiyagarajan, P.; Colby, R. H.; Douglas, J. F. *Nat. Mater.* **2009**, *8*, 354−359. (b) Parab, H.; Jung, C.; Woo, M.-A.; Park, H. G. J. *Nanopart Res.* **2011**, *13*, 2173−2180. (c) van Herrikhuyzen, J.; Janssen, R. A. J.; Meijer, E. W.; Meskers, S. C. J.; Schenning, A. P. H. J. *J. Am. Chem. Soc.* **2006**, *128*, 686−687.

(2) (a) Ye, W. C.; Yan, J. F.; Ye, Q.; Zhou, F. *J. Phys. Chem. C* **2010**, *114*, 15617−15624. (b) Joseph, D.; Geckeler, K. E. *Langmuir* **2009**, *25*,

13224−13231. (c) Tang, X. L.; Jiang, P.; Ge, G. L.; Tsuji, M.; Xie, S. S.; Guo, Y. J. *Langmuir* **2008**, *24*, 1763−1768. (d) Bai, X. T.; Gao, Y. A.; Zheng, L. Q. *CrystEngComm* **2011**, *13*, 3652−3568.
(3) (a) Mohanty, A.; Garg, N.; Jin, R. C. *Angew. Chem.* **2010**, *122*, 5082−5086. (b) Bai, X. T.; Zheng, L. Q. *Cryst. Growth Des.* **2010**, *10*, 4701−4075.
(4) Han, X. Y.; Wang, D. W.; Huang, J. S.; Liu, D.; You, T. Y. *J. Colloid Interface Sci.* **2011**, *354*, 577−584.
(5) (a) Martin, H.; Carro, P.; Creus, A. H.; Conzalez, S.; Andreasen, G.; Salvarezza, R. C.; Arvia, A. J. *Langmuir* **2000**, *16*, 2915−2923. (b) Tian, N.; Zhou, Z. Y.; Sun, S. G.; Cui, L.; Ren, B.; Tian, Z. Q. *Chem. Commun.* **2006**, 4090−4092. (c) Geddes, C. D.; Parfenov, A.; Gryczynski, I.; Lakowicz, J. R. *J. Phys. Chem. B* **2003**, *107*, 9989−9993.
(6) (a) Fang, J. X.; Ma, X. N.; Cai, H. H.; Song, X. P.; Ding, B. J. *Nanotechnology* **2006**, *17*, 5841−5845. (b) Qin, Y.; Song, Y.; Sun, N. J.; Zhao, N. N.; Li, M. X.; Qi, L. M. *Chem. Mater.* **2008**, *20*, 3965−3972.
(7) (a) Zheng, X.; Zhu, L.; Wang, X.; Yan, A.; Xie, Y. J. *Cryst. Growth* **2004**, *260*, 255−262. (b) Pan, M.; Xing, S.; Sun, T.; Zhou, W.; Sindoro, M.; Teo, H. H.; Yanb, Q.; Chen, H. *Chem. Commun.* **2010**, *46*, 7112−7114. (c) Xu, X.; Jia, J.; Yang, X.; Dong, S. *Langmuir* **2010**, *26*, 7627−7631.
(8) (a) Wang, Y. L.; Camargo, P. H. C.; Skrabalak, S. E.; Gu, H. C.; Xia, Y. N. *Langmuir* **2008**, *4*, 12042−12046. (b) Sun, X. P.; Hagner, M. *Langmuir* **2007**, *23*, 9147−9150. (c) Fang, J. X.; You, H. J.; Kong, P.; Yi, Y.; Song, X. P.; Ding, B. J. *Cryst Growth Des* **2007**, *7*, 864−867.
(9) (a) Nittmann, J.; Stanley, H. E. *Nature* **1986**, *321*, 663−668. (b) Ben-Jacob, E.; Garik, P. *Nature* **1990**, *343*, 523−530.
(10) Viswanath, B.; Kundu, P.; Halder, A.; Ravishankar, N. *J. Phys. Chem. C* **2009**, *113*, 16866−16883.
(11) Xiao, J. Y.; Qi, L. M. *Nanoscale* **2011**, *3*, 1383−1396.
(12) (a) Kumar, P. S.; Pastoriza-Santos, I.; Rodríguez-González, B.; García de Abajo, F. J.; Liz-Marzán, L. M. *Nanotechnology* **2008**, *19*, 015606. (b) Wang, X. Q.; Itoh, H.; Naka, K.; Chujo, Y. *Langmuir* **2003**, *19*, 6242−6246. (c) Shen, Q. M.; Jiang, L. P.; Zhang, H.; Min, Q. H.; Hou, W. H.; Zhu, J. J. *J. Phys. Chem. C* **2008**, *112*, 16385−16392. (d) Xiong, Y. J.; Washio, I.; Chen, J. Y.; Cai, H. G.; Li, Z. Y.; Xia, Y. N. *Langmuir* **2006**, *22*, 8563−8570. (e) Li, D.; Cui, X. Y.; Wang, K. W.; He, Q.; Yan, X. H.; Li, J. B. *Adv. Funct. Mater.* **2007**, *17*, 3134−3140.
(13) (a) Ma, Z. F.; Han, H. L. *Colloids Surf., A* **2008**, *317*, 229−233. (b) Zhu, J.; Liao, X.; Chen, H. *Mater. Res. Bull.* **2001**, *36*, 1687−1692. (c) Yan, X. H.; lacklock, J.; Li, J. B.; Mohwald, H. *ACS Nano* **2012**, *6*, 111−117.
(14) (a) Nardelli, A.; Fronzoni, G.; Stener, M. *Phys. Chem. Chem. Phys.* **2011**, *13*, 480−487. (b) Lu, L. H.; Kobayashi, A.; Kikkawa, Y.; Tawa, K.; Ozaki, Y. *J. Phys. Chem. B* **2006**, *110*, 23234−23241.
(15) Xia, Y.; Xiong, Y.; Lim, B.; Skrabalak, S. E. *Angew. Chem., Int. Ed.* **2009**, *48*, 60−103.
(16) Pallavicini, P.; Chirico, G.; Collini, M.; Dacarro, G.; Donà, A.; D'Alfonso, L.; Falqui, A.; Diaz-Fernandez, Y.; Freddi, S.; Garofalo, B.; Genovese, A.; Sironi, L.; Taglietti, A. *Chem. Commun.* **2011**, *47*, 1315−1317.
(17) (a) Ha, T. H.; Koo, H.-J.; Chung, B. H. *J. Phys. Chem. C* **2007**, *111*, 1123−1130. (b) Liu, M.; Guyot-Sionnest, P. *J. Phys. Chem. B* **2005**, *109*, 22192−22200. (c) Shen, Y. F.; Wang, J. B.; Kuhlmann, U.; Hildebrandt, P.; Ariga, K.; Möhwald, H.; Kurth, D. G.; Nakanishi, T. *Chem.—Eur. J.* **2009**, *15*, 2763−2767. (d) Su, Y.; He, Q.; Yan, X.; Fei, J.; Cui, Y.; Li, J. *Chem.—Eur. J.* **2011**, *17*, 3370−3371.
(18) Selvan, S. T.; Hayakawa, T.; Nogami, M.; Mo1ller, M. *J. Phys. Chem. B* **1999**, *103*, 7441−7448.
(19) Borodko, Y.; Habas, S. E.; Koebel, M.; Yang, P.; Frei, H.; Somorjai, G. A. *J. Phys. Chem. B* **2006**, *110*, 23052−23059.
(20) Pang, S. F.; Kondo, T.; Kawai, T. *Chem. Mater.* **2005**, *17*, 3636−3641.
(21) Huang, D. P.; Bai, X. T.; Zheng, L. Q. *J. Phys. Chem. C* **2011**, *115*, 14641−14647.
(22) (a) Fan, L.; Guo, R. *Cryst. Growth Des.* **2008**, *8*, 2150−2156. (b) Lee, J-H; Kamada, K.; Enomoto, N.; Hojo, J. *Chem. Lett.* **2007**, *36*, 728−734. (c) Zhao, N.; Wei, Y.; Sun, N. J.; Chen, Q. J.; Bai, J. W.; Zhou, L. P.; Qin, Y.; Li, M. X.; Qi, L. M. *Langmuir* **2008**, *24*, 991−998. (d) Gao, J. X.; Bender, C. M.; Murphy, C. J. *Langmuir* **2003**, *19*, 9065−9070.
(23) Huang, T.; Meng, F.; Qi, L. M. *Langmuir* **2010**, *26*, 7582−7589.
(24) Zhao, M. W.; Zheng, L. Q. *Phys. Chem. Chem. Phys.* **2011**, *13*, 1332−1337.
(25) (a) Floris, T.; Kluson, P.; Bartek, L.; Pelantova, H. *Appl. Catal., A* **2009**, *366*, 160−165. (b) Kou, X. S.; Zhang, S. Z.; Tsung, C.-K.; Yeung, M. H.; Shi, Q. H.; Stucky, G. D.; Sun, L. D.; Wang, J. F.; Yan, C. H. *J. Phys. Chem. B* **2006**, *110*, 16377−16383.
(26) Bai, X. T.; Gao, Y. A.; Liu, H. G.; Zheng, L. Q. *J. Phys. Chem. C* **2009**, *113*, 17730−17736.
(27) Zeng, Q.; Jiang, X.; Yu, A.; Lu, G. *Nanotechnology* **2007**, *18*, 035708.
(28) Imai, H. *Top. Curr. Chem.* **2007**, *270*, 43−72.
(29) (a) Lindman, S.; Lynch, I.; Thulin, E.; Nilsson, H.; Dawson, K. A.; Linse, S. *Nano Lett.* **2007**, *7*, 914−918. (b) Xia, Y. N.; Halas, N. J. *MRS Bull.* **2005**, *30*, 338−344. (c) Orendorff, C. J.; Gole, A.; Sau, T. K.; Murphy, C. J. *Anal. Chem.* **2005**, *77*, 3261−3266. (d) Nikoobakht, B.; El-Sayed, M. A *J. Phys. Chem. A* **2003**, *107*, 3372−3378.
(30) Yang, M.; Alvarez-Puebla, R.; Hyoung-Sug, K.; Aldeanueva Potel, P.; Liz-Marzan, L. M.; Kotov, N. A. *Nano Lett.* **2010**, *10*, 4013−4019.
(31) Hildebrandt, P.; Stockburger, M. *J. Phys. Chem.* **1984**, *88*, 5935−5944.
(32) Wang, Y.; Chen, H.; Dong, S.; Wang, E. *J. Chem. Phys.* **2006**, *124*, 074709.